

Fluctuation-Induced Friction in Bubble-Wall Dynamics of Cosmological First-Order Phase Transitions

Dongdong Wei^{1,2,3*} and Zong-Kuan Guo^{3,2,1†}

¹*School of Fundamental Physics and Mathematical Sciences, Hangzhou Institute for Advanced Study, University of Chinese Academy of Sciences, Hangzhou 310024, China*

²*School of Physical Sciences, University of Chinese Academy of Sciences, No.19A Yuquan Road, Beijing 100049, China*

³*Institute of Theoretical Physics, Chinese Academy of Sciences, Beijing 100190, China*

(Dated: February 5, 2026)

We study bubble-wall dynamics in cosmological first-order phase transitions in a two-scalar-field model, where the wall is formed by ϕ and an additional real scalar s couples through a portal interaction. We evolve the coupled classical field equations on the lattice and demonstrate that for an initial Bose-Einstein distribution of s fluctuations at the nucleation temperature T_n , the resulting patchy background intermittently modulates the local driving pressure on the wall. The wall therefore undergoes alternating episodes of acceleration and deceleration and approaches a quasi-stationary propagation regime with a smaller time-averaged speed than in the decoupled limit. We further identify three familiar propagation profiles—deflagration, detonation, and hybrid—distinguished by where the dynamical s -sector energy density is concentrated relative to the wall. These effects can impact gravitational-wave and baryogenesis predictions.

Introduction. Cosmological first-order phase transitions (FOPTs) proceed through the nucleation and expansion of bubbles of the broken phase. They are a well-motivated source of a stochastic gravitational wave (GW) background and a central ingredient in many baryogenesis scenarios, making their real-time dynamics an important target for both theory and upcoming space-based GW observatories such as LISA, Taiji, and TianQin[1–6]. A key parameter controlling these phenomena is the bubble-wall velocity: it affects the efficiency and duration of acoustic GW sources, the partition of released vacuum energy into bulk motion versus field gradients, and—at the electroweak scale—the viability of charge transport ahead of the wall.[7–12].

Bubble-wall propagation in cosmological FOPTs is driven by the free-energy (pressure) difference between phases and opposed by the cumulative backreaction of the surrounding medium and any additional coupled degrees of freedom. If this backreaction is insufficient to balance the driving pressure, the wall can continue to gain kinetic energy and approach an ultra-relativistic, near-luminal regime (a “runaway” behavior) [13]. Such fast walls have important phenomenological implications: for electroweak baryogenesis they tend to suppress CP-asymmetric charge diffusion ahead of the wall, since the relevant diffusion length in the wall frame decreases as the relative wall-plasma speed increases [11]; meanwhile, for GW predictions they modify how the released vacuum energy is apportioned between scalar-field gradients and bulk plasma motion, thereby impacting the resulting signal [7–9, 14].

A variety of approaches have therefore been developed to determine, or effectively bound, the wall velocity by incorporating backreaction in a controlled way. Semiclassical transport calculations extract an effective friction from departures of particle distributions from equilibrium in the moving-wall background, typically by solving (or moment-expanding) Boltzmann equations, and can yield both the wall speed and wall thickness in electroweak-scale settings [15]. Even within local thermal equilibrium, hydrodynamic backreaction can obstruct acceleration: compression heating in front of the interface reduces the effective driving and can enforce subsonic propagation under a simple sufficient criterion [16]; real-time simulations under the assumption of *local thermal equilibrium* confirm that purely hydrodynamic backreaction can lead to steady-state expansion in appropriate regimes [17]. A widely used numerical realization of this physics is the scalar–fluid framework[18, 19], where the scalar field is evolved together with a relativistic fluid and their interaction is encoded via a phenomenological damping coefficient; this framework underlies state-of-the-art 3D simulations of bubble growth and the associated GW source [7].

Motivated by these developments, we explore a complementary slowdown mechanism that does not rely on introducing a phenomenological fluid-friction term. Instead of modeling the ambient medium as a relativistic fluid coupled to the wall, we represent it by an additional scalar degree of freedom coupled to the wall through a portal interaction. Following the classical-statistical strategy used in real-time vacuum-decay simulations, we evolve the coupled classical field equations with an initial Bose-Einstein distribution of fluctuations for the extra scalar [20]. The resulting stochastic inhomogeneities provide a patchy background that modulates the local

* weidd@ucas.ac.cn

† guozk@itp.ac.cn

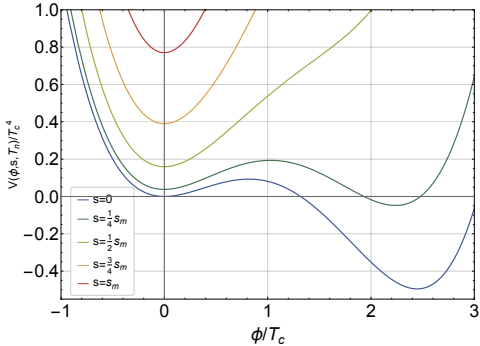


FIG. 1. Potential slices $V(\phi, s, T_n)$ as functions of ϕ/T_c at the nucleation temperature T_n , evaluated for five fixed values of s (see legend). Model parameters are the same as in Table I, and $\lambda_{\phi s} = 1$.

free-energy release—and hence the driving pressure on the wall—from patch to patch. This leads to intermittent episodes of acceleration and deceleration and can obstruct sustained wall acceleration. We demonstrate the effect with three-dimensional lattice simulations of expanding spherical bubbles, and then use complementary 1 + 1 dimensions simulations to clarify the underlying mechanism and to classify deflagration-, detonation-, and hybrid-like profiles from the spatial distribution of the s -sector dynamical energy relative to the wall.

Model. We study bubble-wall dynamics in a two-scalar-field model, where ϕ controls the phase transition and s is a thermally populated scalar coupled through a portal interaction. Motivated by generic renormalizable scalar-portal extensions (e.g., singlet-extended Higgs sectors and their multi-singlet generalizations), we employ the standard high-temperature parametrization of the finite-temperature effective potential for two real scalars [21–24]:

$$V(\phi, s, T) = \frac{m_\phi^2(T)}{2} \phi^2 + \frac{\lambda_\phi}{4} \phi^4 + \frac{\mu_3}{2\sqrt{2}} \phi^3 + \frac{m_s^2(T)}{2} s^2 + \frac{\lambda_s}{4} s^4 + \frac{\lambda_{\phi s}}{4} \phi^2 s^2, \quad (1)$$

where $m_\phi^2(T)$ and $m_s^2(T)$ are the temperature-dependent mass parameters (including thermal corrections), λ_ϕ and λ_s are the quartic self-couplings of ϕ and s , respectively, μ_3 is the (dimensionful) cubic coupling of ϕ , and $\lambda_{\phi s}$ is the portal coupling between ϕ and s .

For an initial Bose–Einstein distribution of s fluctuations at T_n , the ensuing real-time evolution yields a patchy $s(\mathbf{x}, t)$ background; via the portal coupling $\lambda_{\phi s}$ the wall samples a distribution of local s values, typically near 0 but with rare excursions up to s_m (the maximum observed in our simulations). As illustrated in Fig. 1, such excursions modify the potential profile along the ϕ direction, i.e., the location and depth of the ϕ minima of $V(\phi, s, T)$ evaluated at $s = s_m$ or

$s = 0$. Equivalently, the local free-energy difference $\Delta V(s) \equiv V(\phi_{\text{false}}, s, T) - V(\phi_{\text{true}}, s, T)$, which provides the driving pressure on the wall, becomes patch dependent. In regions with $s \simeq s_m$, the would-be broken-phase minimum along ϕ can become metastable (a false vacuum), thereby strongly suppressing the driving pressure; the wall can then decelerate or even transiently stall. Conversely, for $s \simeq 0$ the portal contribution $\propto \phi^2 s^2$ is smaller than in regions with $s \simeq s_m$, so the suppression of the local driving free-energy difference ΔV is alleviated and the wall can re-accelerate. Nevertheless, since the portal term is even in s , any nonzero s still modifies ΔV , implying that the acceleration is typically weaker than in the unperturbed case.

As a result, the wall dynamics becomes intermittent: it undergoes alternating episodes of acceleration and deceleration as it samples different s -patches. Over length scales larger than the typical fluctuation correlation length, these episodes average out and the wall approaches an effectively steady propagation. This quasi-stationary regime can be viewed as a dynamical balance between the driving force set by the (patch-averaged) potential difference and the dissipative backreaction induced by the coupling to s . Consequently, after a short transient the wall reaches an approximately constant terminal speed, while its instantaneous velocity continues to fluctuate around the mean. A closely related recent lattice study has highlighted a complementary possibility: for a *mass-acquiring* spectator scalar, the field amplitude can be strongly suppressed inside true-vacuum bubbles, which triggers an additional release of vacuum energy that accumulates on the bubble wall and can enhance the transition strength and the GW source [25]. By contrast, we emphasize the opposite effect in the classical-statistical evolution with an initial Bose–Einstein distribution of s fluctuations: the ensuing stochastic spatial inhomogeneities can intermittently *suppress* the local driving pressure, obstructing sustained wall acceleration and leading to an intermittent quasi-stationary propagation regime.

To validate the above picture, we perform real-time lattice simulations of the coupled (ϕ, s) system. We evolve the classical field equations on a cubic grid with $N^3 = 2000^3$ sites and physical size $LT_c = 400$, corresponding to a lattice spacing $dx T_c = 0.2$. The time step is chosen as $dt = 0.2 dx$. Spatial derivatives are discretized using a second-order central-difference scheme, and the time evolution is carried out with a leapfrog integrator, which is second order in dt and well suited for long-time Hamiltonian evolution.

The real-time dynamics of the two coupled scalar fields

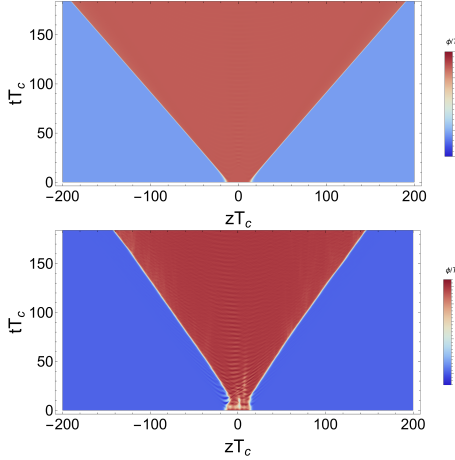


FIG. 2. Spacetime evolution of the field ϕ along the z axis. We show the line-out $\phi(t, z)$ taken on the central slice ($x = y = 0$), i.e., along the z axis through the bubble center. Top: vanishing portal coupling, $\lambda_{\phi s} = 0$. Bottom: finite coupling, $\lambda_{\phi s} = 7.5$.

TABLE I. Benchmark parameters used in the simulations.

Model	$m_\phi(T)/T_c$	λ_ϕ	$m_s(T)/T_c$	μ_3/T_c	λ_s	T_n/T_c	R_0	ℓ_w
	M_2	1	0.5	1	-0.578	0.5	0.8	14.15 1.71

is governed by the classical equations of motion,

$$\ddot{\phi}(t, \mathbf{x}) - \nabla^2 \phi(t, \mathbf{x}) + \frac{\partial V(\phi, s, T)}{\partial \phi} = 0, \quad (2)$$

$$\ddot{s}(t, \mathbf{x}) - \nabla^2 s(t, \mathbf{x}) + \frac{\partial V(\phi, s, T)}{\partial s} = 0, \quad (3)$$

where $\nabla^2 \equiv \partial_x^2 + \partial_y^2 + \partial_z^2$ and $V(\phi, s, T)$ is given in Eq. (1). For the simulations, we adopt the benchmark parameters listed in Table I. At the nucleation temperature T_n , we embed at the box center a spherical bubble profile at the critical radius, representing a nucleated critical bubble. Writing $r \equiv |\mathbf{x} - \mathbf{x}_0|$ with \mathbf{x}_0 the box center, we take

$$\begin{aligned} \phi(t = 0, \mathbf{x}) &= \phi_{\text{false}} + \frac{\phi_{\text{true}} - \phi_{\text{false}}}{2} \left[1 - \tanh\left(\frac{r - R_0}{\ell_w}\right) \right], \\ \dot{\phi}(t = 0, \mathbf{x}) &= 0, \end{aligned} \quad (4)$$

where ϕ_{false} and ϕ_{true} denote the field values in the outside (metastable) and inside (broken) phases, respectively. The wall thickness ℓ_w is taken from the critical-bubble (bounce) solution at T_n , while the initial radius R_0 is treated as a tunable parameter: in practice we choose R_0 slightly above the critical radius to ensure outward growth in the presence of fluctuations and to facilitate a clean exploration of the wall dynamics.

The stochasticity of the s field is encoded in the initial ensemble. Following the classical-stochastic strategy with an initial Bose-Einstein distribution of fluctuations

at T_n , we decompose s into a homogeneous background plus fluctuations,

$$s(t=0, \mathbf{x}) = \bar{s} + \delta s(\mathbf{x}), \quad \dot{s}(t=0, \mathbf{x}) = \delta \dot{s}(\mathbf{x}), \quad (5)$$

and sample the Fourier modes $\delta s_{\mathbf{k}}$ and $\delta \dot{s}_{\mathbf{k}}$ as Gaussian random variables with variances chosen to reproduce Bose-Einstein mode occupancies,

$$\langle |\delta s_{\mathbf{k}}|^2 \rangle = \frac{n_{\mathbf{k}}}{\omega_{\mathbf{k}}}, \quad \langle |\delta \dot{s}_{\mathbf{k}}|^2 \rangle = n_{\mathbf{k}} \omega_{\mathbf{k}}, \quad (6)$$

where $n_{\mathbf{k}} = [\exp(\omega_{\mathbf{k}}/T_n) - 1]^{-1}$ and $\omega_{\mathbf{k}}^2 = \mathbf{k}^2 + m_s^2(T_n)$. The real-field condition is enforced by $\delta s_{-\mathbf{k}} = \delta s_{\mathbf{k}}^*$ (and similarly for $\delta \dot{s}_{\mathbf{k}}$).

Figure 2 contrasts the portal-decoupled limit ($\lambda_{\phi s} = 0$, top) with the portal-coupled dynamics (bottom). In the decoupled case, the bubble expands more rapidly: at fixed time the wall reaches a larger radius than in the coupled case. The ϕ profile inside the bubble is comparatively smooth, exhibiting only small-amplitude post-wall oscillations about the broken-phase minimum. Once the portal coupling is switched on (bottom, $\lambda_{\phi s} = 7.5$), the expansion is visibly hindered and the wall advance is reduced. In addition, the interior profile develops more pronounced oscillations, consistent with a sustained energy exchange between ϕ and the additional dynamical degree of freedom s . Remarkably, at early times the bubble can undergo a transient contraction followed by re-expansion, indicating that the local driving free-energy difference can be temporarily suppressed by the s -induced back-reaction. Such a shrink-reexpand behavior is absent in the standard uncoupled first-order transition dynamics. It is also instructive to contrast our mechanism with the widely used scalar-fluid description, in which the field ϕ is coupled to a relativistic plasma through a phenomenological friction (damping) term in the scalar equation of motion. In that framework, the coupling acts as a dissipative channel that efficiently transfers scalar kinetic/gradient energy into bulk fluid motion, so the field ϕ typically relaxes quickly behind the wall and post-transition oscillations are strongly damped. The persistence—and even enhancement—of interior oscillations in our two-scalar setup therefore points to a qualitatively different origin of the wall slowdown: a fluctuation-induced, spatially inhomogeneous modulation of the effective potential rather than fluid-like viscous damping.

To quantify the wall motion in Fig. 2, we track the instantaneous wall position using a field-based isosurface criterion. At each time slice we define a tracer value as the midpoint between the false- and true-vacuum values of the ϕ , $\phi_* \equiv (\phi_{\text{false}} + \phi_{\text{true}})/2$, and determine the wall location $z_w(t)$ from the condition $\phi(t, z_w) = \phi_*$ along the z axis. The wall velocity is then obtained from a finite-difference estimate $v(t) \simeq [z_w(t + \Delta t) - z_w(t - \Delta t)]/(2\Delta t)$. The resulting velocity histories are shown in Fig. 3. For the uncoupled case $\lambda_{\phi s} = 0$ (black), the wall accelerates rapidly and approaches $v \simeq 0.976$ by $tT_c \simeq 200$.

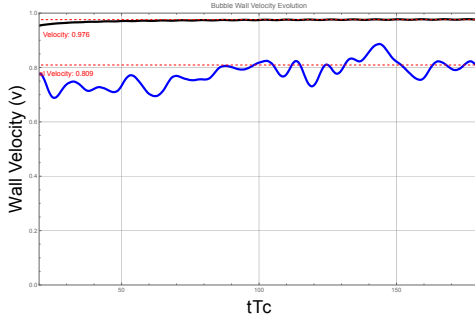


FIG. 3. Bubble-wall velocity evolution extracted from the isosurface condition $\phi_* \equiv (\phi_{\text{false}} + \phi_{\text{true}})/2$. Black solid: $\lambda_{\phi s} = 0$. Blue solid: $\lambda_{\phi s} = 7.5$. The horizontal red dashed lines indicate the corresponding terminal velocities estimated at $tT_c = 200$.

This near-luminal saturation is consistent with the absence of any additional backreaction channel: in practice, once the wall becomes highly relativistic, its Lorentz-contracted thickness can approach the lattice resolution, and the leapfrog/central-difference discretization introduces numerical dispersion that can bias the measured propagation speed slightly below unity. In contrast, for $\lambda_{\phi s} = 7.5$ (blue) the wall velocity remains strongly time dependent, fluctuating around $v \simeq 0.8$ with no clear secular drift, reflecting alternating acceleration and deceleration as the wall traverses s -fluctuation patches. Overall, the coupled case exhibits an intermittent regime: thermal fluctuations of s make the local driving pressure patch dependent, while the portal interaction continuously feeds energy into s excitations, resulting in a quasi-stationary terminal speed with persistent fluctuations rather than sustained acceleration.

Energy Distribution. To establish a clear classification of the bubble-wall profile, we analyze the coupled dynamics in $1+1$ dimensions. This reduced setup enables long-time evolutions and efficient scans over the portal coupling, making it well suited for resolving the wall-scale energy deposition that distinguishes the three types. We have verified that the corresponding $3+1$ dimensional simulations exhibit the same qualitative behavior, indicating that the dimensional reduction does not alter the essential physics. The total energy density is

$$\rho_{\text{tot}}(t, x) = \frac{1}{2}\dot{\phi}^2 + \frac{1}{2}(\partial_x \phi)^2 + \frac{1}{2}\dot{s}^2 + \frac{1}{2}(\partial_x s)^2 + V(\phi, s, T). \quad (7)$$

While to quantify the energy carried by propagating s excitations we focus on the **dynamical** contribution,

$$\rho_s(t, x) \equiv \frac{1}{2}\dot{s}^2 + \frac{1}{2}(\partial_x s)^2. \quad (8)$$

This choice avoids the bookkeeping ambiguity of assigning interaction/potential-energy contributions to individual fields and cleanly captures where the s -sector excitations are localized relative to the wall. Within this

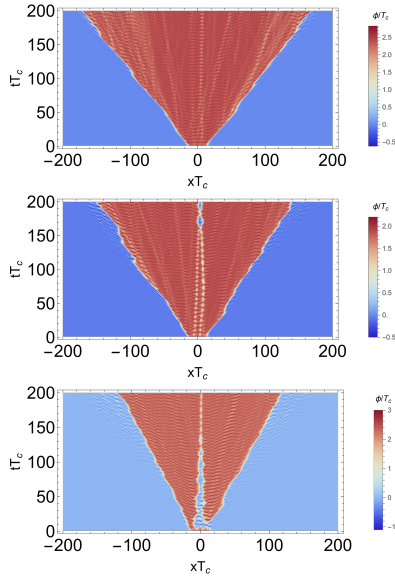


FIG. 4. Time evolution of a vacuum bubble in the two-scalar-field system. The simulation volume and discretization are $LT_c = 500$, $dx T_c = 0.1$, and $dt = 0.2 dx$. The parameters entering $V(\phi, s, T)$ are chosen to match the benchmark point used in the $3+1$ dimensions simulations, while the portal coupling is varied as $\lambda_{\phi s} = 0.65, 1.1$, and 1.8 from top to bottom.

reduced framework, we scan the portal coupling $\lambda_{\phi s}$ and, correspondingly, the resulting wall-speed behavior (set by the balance between the driving pressure and interaction-induced backreaction/friction). We identify three characteristic regimes, in analogy with the familiar hydrodynamic classification into deflagrations, detonations, and hybrids[26], distinguished by where ρ_s is concentrated relative to the direction of wall propagation: (i) a deflagration-like profile, with ρ_s predominantly building up ahead of the wall; (ii) a detonation-like profile, with ρ_s concentrated behind the wall; and (iii) a hybrid profile, with comparable support both in front of and behind the wall.

The dynamics of the coupled scalar fields are governed by the equations:

$$\begin{aligned} \ddot{\phi}(x, t) - \partial_x^2 \phi(x, t) + \frac{\partial V(\phi, s, T)}{\partial \phi} &= 0, \\ \ddot{s}(x, t) - \partial_x^2 s(x, t) + \frac{\partial V(\phi, s, T)}{\partial s} &= 0. \end{aligned} \quad (9)$$

We initialize the $1+1$ dimensional system at $t = 0$ by embedding the critical-bubble profile of ϕ at T_n along x and by sampling the s field (and \dot{s}) from an initial Bose-Einstein distribution of fluctuations at T_n . This stochastic initialization generates an inhomogeneous $s(x, 0)$ background already in $1+1$ dimensions.

From Fig. 4, we observe that different values of the coupling $\lambda_{\phi s}$ significantly influence the bubble wall velocity. In the top panel, where the coupling is small, fluctuations

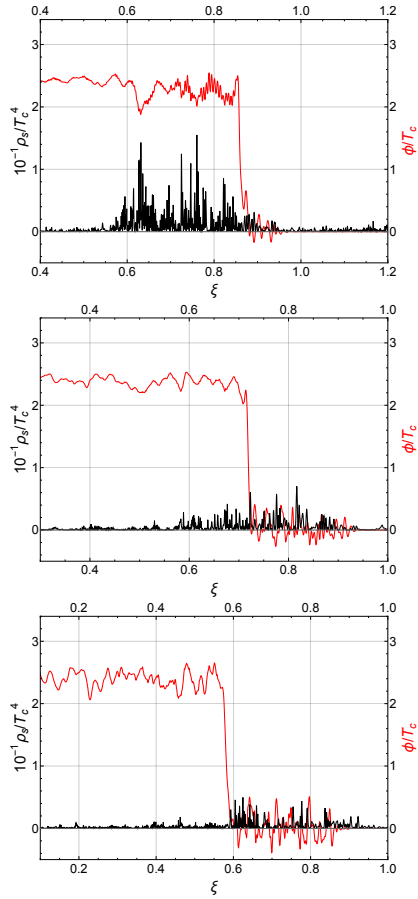


FIG. 5. Profiles of the s dynamical energy density (left axis, $10^{-1}\rho_s/T_c^4$) and the field ϕ/T_c at the fixed time $tT_c = 180$, shown as functions of the coordinate $\xi \equiv x/t$. In this representation ξ plays the role of a velocity coordinate (in units of c), so the wall position directly visualizes the propagation speed. From top to bottom the portal coupling is $\lambda_{\phi s} = 0.65$, 1.1, and 1.8 (other potential parameters are kept fixed).

of the s field exert minimal influence on the s field, allowing the bubble wall to propagate at a speed approaching the speed of light. As $\lambda_{\phi s}$ increases (e.g., to 1.1), the wall velocity gradually decreases to approximately $v \sim 0.7$. Beyond a certain threshold in our model, the wall can no longer expand — its minimal attainable velocity is around $v \sim 0.6$ — and the vacuum bubble ultimately collapses. Interestingly, within the parameter range that supports bubble expansion, no fine-tuning of $\lambda_{\phi s}$ allows the wall velocity to drop below $v \sim 0.6$. We interpret this behavior as arising from the significant modification of the vacuum structure by the larger coupling parameter, which effectively imposes a lower bound on the wall velocity in this model.

In Fig. 5 we show the profile of the field ϕ and the ρ_s at a given time. The resulting the dynamical part of the energy-density distribution resemble patterns commonly associated with deflagration, detonation, or hybrid modes in scalar-fluid systems, the detailed behavior

in our two-scalar model differs significantly from any of these standard hydrodynamic templates. First, no sharp shock front or discontinuity in the energy density is observed ahead of the wall. This may partly stem from the relatively small coupling used in our simulation, which weakens the effective “compression” that would otherwise be present in a fluid. Moreover, the spatial variation of the energy density is not as smooth as in fluid descriptions, because all energy transfer occurs purely through field dynamics. The dynamics of the coupled scalar system are highly nonlinear, and the resulting profiles naturally exhibit fluctuations and local distortions that have no analogue in hydrodynamic treatments. Consequently, even when the macroscopic distribution appears superficially similar to the standard bubble-wall classifications, the microscopic structure of the interface remains qualitatively different from that predicted by scalar-fluid models. Second, in our simulations the case with $v \simeq 0.6$ corresponds to a detonation-like profile according to our ρ_s -based classification. For comparison, in scalar-fluid hydrodynamics $v \simeq 0.6$ is typically associated with detonation or hybrid solutions.

Therefore, although some macroscopic features—such as the wall speed and the broad shape of the energy-density profile—may visually resemble deflagration- or detonation-type behavior, the underlying dynamics of the two-scalar system are fundamentally different.

Summary & Discussion In our real-time simulations, stochasticity is implemented by initializing the fluctuations with a Bose-Einstein distribution, as in recent lattice studies of vacuum decay [20]. This choice is best regarded as a UV-regulated non-equilibrium ensemble for the classical evolution, and similar patchy backgrounds could also originate from inflationary fluctuations of light spectator fields that classicalize after horizon exit. Because the predicted stochastic GW signal from a FOPT depends sensitively on the bubble-wall speed v (which controls the efficiency and the acoustic source), any mechanism that changes v can modify the GW amplitude and potentially its detailed shape.

In summary, we have shown that fluctuations of an additional scalar degree of freedom can act as an effective, *fluctuation-induced* source of drag on expanding bubble walls. In our lattice simulations, turning on the portal coupling prevents monotonic (runaway-like) acceleration: the wall instead propagates in an intermittent manner and settles into a quasi-stationary regime with a reduced time-averaged speed and persistent fluctuations compared to the decoupled limit. The coupled evolution also displays distinctive transients—most notably a shrink-reexpand episode at early times and enhanced oscillations in the wake of the wall—indicating a slowdown mechanism that is qualitatively different from smooth viscous damping in scalar-fluid descriptions. In 1 + 1 dimensional simulations, we further organize the bubble-wall profile into deflagration, detonation, and hybrid-like

profiles according to where the dynamical s -sector energy density is supported relative to the wall, using the terminology in its familiar hydrodynamic sense. These results provide a concrete realization of fluctuation-induced friction capable of obstructing bubble-wall acceleration in cosmological first-order phase transitions.

ACKNOWLEDGEMENTS

We thank Jing Liu for helpful discussions. This work is supported in part by the National Natural Science Foundation of China No. 12235019 and No. 12475067.

[1] P. Amaro-Seoane *et al.* (LISA), Laser Interferometer Space Antenna, (2017), arXiv:1702.00786 [astro-ph.IM].

[2] M. Colpi *et al.* (LISA), LISA Definition Study Report, (2024), arXiv:2402.07571 [astro-ph.CO].

[3] W.-R. Hu and Y.-L. Wu, The Taiji Program in Space for gravitational wave physics and the nature of gravity, *Natl. Sci. Rev.* **4**, 685 (2017).

[4] Z. Luo, Y. Wang, Y. Wu, W. Hu, and G. Jin, The Taiji program: A concise overview, *PTEP* **2021**, 05A108 (2021).

[5] J. Mei *et al.* (TianQin), The TianQin project: current progress on science and technology, *PTEP* **2021**, 05A107 (2021), arXiv:2008.10332 [gr-qc].

[6] J. Luo *et al.* (TianQin), TianQin: a space-borne gravitational wave detector, *Class. Quant. Grav.* **33**, 035010 (2016), arXiv:1512.02076 [astro-ph.IM].

[7] M. Hindmarsh, S. J. Huber, K. Rummukainen, and D. J. Weir, Gravitational waves from the sound of a first order phase transition, *Phys. Rev. Lett.* **112**, 041301 (2014), arXiv:1304.2433 [hep-ph].

[8] J. R. Espinosa, T. Konstandin, J. M. No, and G. Servant, Energy Budget of Cosmological First-order Phase Transitions, *JCAP* **06**, 028, arXiv:1004.4187 [hep-ph].

[9] C. Caprini *et al.*, Detecting gravitational waves from cosmological phase transitions with LISA: an update, *JCAP* **03**, 024, arXiv:1910.13125 [astro-ph.CO].

[10] D. E. Morrissey and M. J. Ramsey-Musolf, Electroweak baryogenesis, *New J. Phys.* **14**, 125003 (2012), arXiv:1206.2942 [hep-ph].

[11] J. M. Cline and K. Kainulainen, Electroweak baryogenesis at high bubble wall velocities, *Phys. Rev. D* **101**, 063525 (2020), arXiv:2001.00568 [hep-ph].

[12] X. Wang, F. P. Huang, and X. Zhang, Phase transition dynamics and gravitational wave spectra of strong first-order phase transition in supercooled universe, *JCAP* **05**, 045, arXiv:2003.08892 [hep-ph].

[13] D. Bodeker and G. D. Moore, Can electroweak bubble walls run away?, *JCAP* **05**, 009, arXiv:0903.4099 [hep-ph].

[14] L. Leitao and A. Megevand, Gravitational waves from a very strong electroweak phase transition, *JCAP* **05**, 037, arXiv:1512.08962 [astro-ph.CO].

[15] G. D. Moore and T. Prokopec, Bubble wall velocity in a first order electroweak phase transition, *Phys. Rev. Lett.* **75**, 777 (1995), arXiv:hep-ph/9503296.

[16] T. Konstandin, G. Nardini, and M. Quiros, Gravitational Backreaction Effects on the Holographic Phase Transition, *Phys. Rev. D* **82**, 083513 (2010), arXiv:1007.1468 [hep-ph].

[17] T. Krajewski, M. Lewicki, and M. Zych, Bubble-wall velocity in local thermal equilibrium: hydrodynamical simulations vs analytical treatment, *JHEP* **05**, 011, arXiv:2402.15408 [astro-ph.CO].

[18] H. Kurki-Suonio and M. Laine, On bubble growth and droplet decay in cosmological phase transitions, *Phys. Rev. D* **54**, 7163 (1996), arXiv:hep-ph/9512202.

[19] J. Ignatius, K. Kajantie, H. Kurki-Suonio, and M. Laine, The growth of bubbles in cosmological phase transitions, *Phys. Rev. D* **49**, 3854 (1994), arXiv:astro-ph/9309059.

[20] D. Pîrvu, M. C. Johnson, and S. Sibiryakov, Bubble velocities and oscillon precursors in first-order phase transitions, *JHEP* **11**, 064, arXiv:2312.13364 [hep-th].

[21] M. Quiros, Finite temperature field theory and phase transitions, in *ICTP Summer School in High-Energy Physics and Cosmology* (1999) pp. 187–259, arXiv:hep-ph/9901312.

[22] S. Profumo, M. J. Ramsey-Musolf, C. L. Wainwright, and P. Winslow, Singlet-catalyzed electroweak phase transitions and precision Higgs boson studies, *Phys. Rev. D* **91**, 035018 (2015), arXiv:1407.5342 [hep-ph].

[23] A. Tofighi, O. N. Ghodsi, and M. Saeedhoseini, Phase transition in multi-scalar-singlet extensions of the Standard Model, *Phys. Lett. B* **748**, 208 (2015), arXiv:1510.00791 [hep-ph].

[24] R. Zhou, J. Yang, and L. Bian, Gravitational Waves from first-order phase transition and domain wall, *JHEP* **04**, 071, arXiv:2001.04741 [hep-ph].

[25] Y.-J. Li, J. Liu, and Z.-K. Guo, Dynamical backreaction of a mass-acquiring scalar field on first-order phase transitions, *Phys. Rev. D* **113**, 023550 (2026), arXiv:2508.14665 [astro-ph.CO].

[26] D. J. Weir, Gravitational waves from a first order electroweak phase transition: a brief review, *Phil. Trans. Roy. Soc. Lond. A* **376**, 20170126 (2018), [Erratum: *Phil. Trans. Roy. Soc. Lond. A* **381**, 20230212 (2023)], arXiv:1705.01783 [hep-ph].